  Bull. Chem. Soc. Jpn., 60, 2641—2650 (1987)

The Reactions of Alkoxyl Radicals with O_2. IV. n-C_4H_9O Radicals†

Paul MORABITO and Julian HEICKLEN*
Department of Chemistry and Center for Air Environment Studies, The Pennsylvania State University, University Park, PA 16802, U.S.A.
(Received December 2, 1985)

n-C_4H_9ONO was photolyzed with 366 nm radiation at −8, 23, 55, 88, and 120 °C in the presence of NO, O_2, and N_2. The quantum yields of n-C_3H_7CHO, C_2H_5CHO, and CH_3CHO were measured as a function of reaction conditions. The primary photolytic act produces n-$C_4H_9O\cdot$ radicals which can react with NO by two routes

$$n\text{-}C_4H_9O\cdot + NO \longrightarrow n\text{-}C_4H_9ONO \quad (2a)$$
$$\longrightarrow n\text{-}C_3H_7CHO + HNO \quad (2b)$$

or isomerize via an internal H-atom abstraction

$$n\text{-}C_4H_9O\cdot \longrightarrow I\cdot \quad (4)$$

where I· is the $HOCH_2CH_2CH_2CH_2\cdot$ radical, and $\ln(k_4/k_2, \text{mol dm}^{-3})=1.93\pm1.60-(4014\pm509)/T$. If k_2 is taken as 2.6×10^{10} dm^3 mol^{-1} s^{-1}, then $\log(k_4, \text{s}^{-1})=11.25\pm0.69-(4014\pm509)/2.303T$. In the presence of O_2, n-$C_4H_9O\cdot$ radicals can also react with O_2

$$n\text{-}C_4H_9O\cdot + O_2 \longrightarrow n\text{-}C_3H_7CHO + HO_2 \quad (6)$$

with $\ln(k_6/k_2)=(-4.09\pm0.54)-(1178\pm176)/T$. If $k_2=2.6\times10^{-10}$ dm^3 mol^{-1} s^{-1}, then $k_6=4.5\times10^8 \exp\{(-1178\pm176)/T\}$ dm^3 mol^{-1} s^{-1}. The radical I· is removed via

$$I\cdot \longrightarrow CH_3CHO + 2CH_2O + HO \quad (12a)$$
$$\longrightarrow \text{Undetected aldehydes} + HO \quad (12b)$$
$$I\cdot + O_2 \longrightarrow n\text{-}C_3H_7CHO + HO \quad (13a)$$
$$\longrightarrow C_2H_5CHO + HO \quad (13b)$$

where these reactions are composites of a series of steps. The ratio $k_{13a}/k_{13b}\simeq1.3\pm0.2$ nearly independent of temperature. The ratio k_{12}/k_{13} was not found very accurately, but is $\simeq3\times10^{-3}$ mol dm^{-3}. There was no evidence for the oxidation of I· leading to dioxygenated products.

Alkoxyl radicals are important intermediates in the atmospheric photooxidation of NO to NO_2. These radicals are produced in the atmosphere from the oxidation of hydrocarbons. Over the past few years studies have been undertaken to determine the rate coefficient for the alkoxyl radical oxidation reaction since these reactions have considerable importance in both photochemical smog and combustion.

Extensive rate coefficient studies have been made only for the $CH_3O\cdot$ radical oxidation.[1-9] Only three studies report rate coefficients for the $C_2H_5O\cdot+O_2$ reaction[9-11] while one report is given for higher homologs such as the n-$C_3H_7O\cdot+O_2$[12] and i-$C_4H_9O\cdot+O_2$[13] systems.

In this study, we investigate the reaction of n-$C_4H_9O\cdot+O_2$. Unlike the other radicals that have been studied, the n-$C_4H_9O\cdot$ radical can undergo a rapid intramolecular hydrogen abstraction to form a new radical:

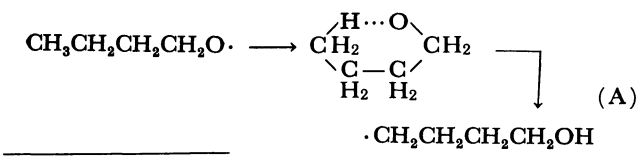

(A)

Such isomerizations are well known in gas phase studies and occur when a δ-carbon atom is present which contains a hydrogen atom.[14] However very few measurements have been made on the isomerization reaction (A) because both reactant and product are free radicals.

The radical produced in step A could now decompose, or in the presence of O_2 and NO, form a new alkoxyl radical, $HO(CH_2)_4O\cdot$. This radical would have a variety of reaction paths available to it and has been subjected to speculation.[15] There are only three experimental studies which report processes involving the isomerization pathway.[16-18] Unfortunately these studies lack detailed qualitative and quantitative information concerning the isomerization pathway. The Arrhenius expressions for reaction A were estimated to be $k_A=10^{11.8}\exp(-8900/RT)$ and $k_A=10^{11.4}\exp(-7700/RT)$ s^{-1}, respectively, by Carter et al.[16] and Baldwin and Golden,[17] where the activation energies are in cal mol^{-1} (1 cal=4.184 J). Niki et al.[18] showed that at 298 K in 700 Torr (1 Torr=133.322 Pa) of air the ratio of reaction of n-$C_4H_9O\cdot$ with O_2 compared to isomerization was 0.23. In this study we not only report the rate coefficient for n-$C_4H_9O\cdot$ isomerization reaction but also report some of the

† CAES Report No. 744-85.

products that are formed from the isomerization pathway.

Experimental

Mixtures of n-C_4H_9ONO with NO, O_2, and N_2 were photolyzed with 366 nm radiation, and the products analyzed using gas chromatography and mass spectrometry. In the gas chromatography system, two reaction cells were used. A 765-cm^3 spherical Pyrex reaction vessel was used for the temperature range of 23 to 120 °C. The reaction vessel was enclosed in an aluminum furnace, resistively-heated in which temperature regulation was achieved by an Omega proportional temperature controller model type 1522. For low-temperature photolysis at −8 °C, a 413 cm^3 cylindrical Pyrex reaction vessel was used. The low temperature was obtained by circulating ethanol cooled by dry ice through a Pyrex jacket that surrounds the reaction vessel. This procedure has been previously described.[11]

After irradiation was terminated, n-C_3H_7CHO, C_2H_5CHO, and CH_3CHO were analyzed on a Varian 1520B gas chromatograph using a FID detector. The products were separated using a 9-foot by 1/4″-diameter stainless-steel column containing GP 20%, SP-2100/0.1% Carbowax 1500 on Supelcoport. All analyses were carried out at 23 °C with a helium flow rate of 25 $cm^3\ min^{-1}$. In experiments with added NO, N_2, or O_2 the excess reactants were removed by condensing a portion of the photolysis mixture in a gas sample loop at −196 °C and pumping off the non-condensable gases prior to analysis.

In the mass spectrometry system a 329-cm^3 cylindrical Pyrex reaction vessel was used for the temperature range of 23 to 120 °C. The heating and regulation of the cell temperature was the same as mentioned earlier. Photolyses at −8 °C were not performed using the mass spectrometer due to the difficulty involved in adapting the low temperature cell to the instrument. The performance and operating parameters of the mass spectrometer have been described in previous studies.[19-20]

In both systems a conventional Pyrex vacuum line was employed. The line was kept grease free by the use of Teflon stopcocks with Viton "O" rings. The source of radiation was a medium pressure mercury lamp (Hanovia type 30620), used in conjunction with a 0—52 and 7—54 Corning glass filters to isolate the 366 nm line.

Quantum yields were based on light intensities measured by the photolysis of azomethane which has also been previously described.[19] The azomethane was prepared as before.[19] Absorption cross-sections were determined by using the lamp/filter combination as a light source and an RCA 935 phototube to measure the radiation. The absorption cross-sections were found to be (to base 10) 5.94×10^{-20} cm^2 for n-C_4H_9ONO which was independent of temperature from −8 to 120 °C and 4.54×10^{-21} cm^2 for azomethane at 23 °C.

The butyl nitrite was prepared as before and stored over mercury and Drierite in the dark at −196 °C.[19] Ninety-nine percent acetaldehyde, propionaldehyde, and butyraldehyde were obtained from Aldrich and used without purification. Extra dry oxygen (>99.6%) was obtained from Airco and used without purification. Matheson NO and N_2 was used; only the NO was purified trap-to-trap from −186 to −196 °C prior to use. All compounds condensable at −196 °C were degassed at this temperature before use.

Results

n-C_4H_9ONO was photolyzed by 366-nm radiation in the presence of NO, N_2, and O_2. The photolysis products n-C_3H_7CHO, C_2H_5CHO, and CH_3CHO were measured. In experiments performed at 88 and 120 °C, product growth occurred even without irradiation. At these elevated temperatures the thermal decomposition of the nitrite starts to become significant thus explaining the dark growth. To obtain correct quantum yields at these temperatures each photolysis was performed along with an identical dark run in which the dark growth was subtracted from the photolytic run. The correction was usually small and always less than 15% of the total amount of each product produced.

Initially experiments were performed in the absence of O_2 with a constant pressure of NO and the total pressure was varied by the addition of N_2. The results are presented in Table 1. At 23 °C, the total density was varied from $\simeq2.8\times10^{-4}$ n-C_4H_9ONO mol dm^{-3} (≈5.0 Torr) to 1.7×10^{-2} mol dm^{-3} (300 Torr) while the concentration of NO and n-C_4H_9ONO remained constant at $\simeq1.6\times10^{-7}$ NO mol dm^{-3} (≈30 mTorr) and 2.8×10^{-4} n-C_4H_9ONO mol dm^{-3} (≈5.0 Torr) respectively. The quantum yield of C_3H_7CHO, $\Phi\{n$-$C_3H_7CHO\}$, essentially remained constant over the entire pressure range, and was equal to 0.012±0.001.

As the temperature increases from −8 to 120 °C, the value of $\Phi\{n$-$C_3H_7CHO\}$ at low NO pressures decreases. However if additional NO is added the value of $\Phi\{n$-$C_3H_7CHO\}$ increases to the same limiting value at high [NO] for every temperature. These results are presented in Table 2. Experiments were performed at constant total pressure of 400 Torr while the NO pressure was varied from ≈30 mTorr to ≈55 Torr.

We next introduced oxygen into our system. First mixtures of n-C_4H_9ONO, NO, and O_2 were photolyzed to illustrate the effect of irradiation time on $\Phi\{n$-

Table 1. Effect of Total Gas Density on the Photolysis of n-C_4H_9ONO-NO Mixtures[a]

Total density[b]/10^{-4} mol dm^{-3}	$\Phi\{n$-$C_3H_7CHO\}$
2.8	0.011
27.4	0.013
54.6	0.012
82.0	0.011
109.4	0.012
164.0	0.011

a) $I_a=7.08\times10^{-5}$ Einsteins/s-mol n-C_4H_9ONO, [NO]=$(1.62\pm0.03)\times10^{-6}$ mol dm^{-3}, T=23 °C, irradiation time=45.00 min, [n-C_4H_9ONO]=$(2.77\pm0.05)\times10^{-4}$ mol dm^{-3}. b) Diluent is N_2.

Table 2. Effect of NO Concentration on the Photolysis of n-C_4H_9ONO-NO Mixtures at 400 Torr Total Pressure[a)]

$[NO]/10^{-6}$ mol cm^{-3}	Irradiation time/min	$\Phi\{n\text{-}C_3H_7CHO\}$
$T=-8$ °C, low temp cell, $I_a=6.87\times10^{-5}$ Einsteins/s-mol n-C_4H_9ONO, $[n\text{-}C_4H_9ONO]=(3.02\pm0.10)\times10^{-4}$ mol dm^{-3}, Total density $=2.42\times10^{-2}$ mol dm^{-3}		
1.88	10.00	0.025
6.13	10.00	0.036
15.16	12.00	0.049
32.5	12.00	0.052
66.7	8.00	0.054
114.6	10.00	0.057
$T=23$ °C, high temp cell, $I_a=7.08\times10^{-5}$ Einsteins/s-mol n-C_4H_9ONO, $[n\text{-}C_4H_9ONO]=(2.74\pm0.08)\times10^{-4}$ mol dm^{-3}, Total density $=2.16\times10^{-2}$ mol dm^{-3}		
2.82	15.00	0.014
6.28	12.00	0.023
13.42	12.00	0.033
26.9	12.00	0.037
50.5	12.00	0.047
102.3	12.00	0.052
140.8	10.00	0.052
553	12.00	0.054
1710	10.00	0.054
$T=55$ °C, high temp cell, $I_a=1.08\times10^{-4}$ Einsteins/s-mol n-C_4H_9ONO, $[n\text{-}C_4H_9ONO]=(2.51\pm0.08)\times10^{-4}$ mol dm^{-3}, Total density $=1.96\times10^{-2}$ mol dm^{3}		
3.75	20.00	0.008
7.22	12.00	0.009
16.04	10.00	0.016
24.7	10.00	0.030
49.8	8.00	0.037
98.1	8.00	0.050
264	7.00	0.059
272	7.00	0.059
$T=88$ °C, high temp cell, $I_a=1.10\times10^{-4}$ Einsteins/s-mol n-C_4H_9ONO, $[n\text{-}C_4H_9ONO]=(2.24\pm0.07)\times10^{-4}$ mol dm^{-3}, Total density $=1.78\times10^{-2}$ mol dm^{-3}		
2.22	25.00	0.001
6.16	15.00	0.003
13.64[b)]	12.00	0.011
22.4	10.00	0.015
45.7	10.00	0.022
94.5	8.00	0.034
239[c)]	8.00	0.051
$T=120$ °C, high temp cell, $I_a=1.14\times10^{-4}$ Einsteins/s-mol n-C_4H_9ONO, $[n\text{-}C_4H_9ONO]=(2.04\pm0.08)\times10^{-4}$ mol dm^{-3}, Total density $=1.63\times10^{-2}$ mol dm^{-3}		
20.8	20.00	0.0023
41.7	15.00	0.0047
77.5	10.00	0.0073
206	8.00	0.012
628	10.00	0.037
910	6.00	0.044
1680	5.00	0.050
2260	5.00	0.051

a) Mixtures brought to total density by adding N_2. b) $[n\text{-}C_4H_9ONO]=1.88\times10^{-4}$ mol dm^{-3}. c) $[n\text{-}C_4H_9ONO]=2.03\times10^{-4}$ mol dm^{-3}.

$C_3H_7CHO\}$. Photolyses were performed at 23 °C for mixtures containing $\simeq2.8\times10^{-4}$ n-C_4H_9ONO mol dm^{-3} ($\approx$5.0 Torr), $\simeq1.6\times10^{-6}$ NO mol dm^{-3} (30 mTorr), and 5.5×10^{-3} O_2 mol dm^{-3} (100 Torr). These data are presented in Table 3 and show that the quantum yield drops slightly with irradiation time between 1.00 and 5.00 min. However it can be observed from a plot of n-C_3H_7CHO produced vs. irradiation time in Fig. 1 that a nearly linear plot is obtained up to $\approx$5.5 min of irradiation time. This corresponds to the production $\approx$14.0 mTorr of n-C_3H_7CHO. Thus as long as irradiations are short enough to produce $\leqslant$14 mTorr of n-C_3H_7CHO, accurate initial quantum yields will be obtained. In all subsequent runs, the amount of n-C_3H_7CHO produced was kept below this value.

Next a series of runs was performed at five temperatures (−8 °C to 120 °C) in which n-C_4H_9ONO and NO pressures were kept constant at $\approx$5.0 Torr and $\approx$30 mTorr respectively while the O_2 pressure varied from 25 to 200 Torr. In each experiment the total pressure was kept constant at 400 Torr by adding N_2 gas. The general trend at each temperature is that $\Phi\{n\text{-}C_3H_7CHO\}$ and $\Phi\{C_2H_5CHO\}$ increase while

Table 3. Effect of Irradiation Time on the Photolysis of n-C_4H_9ONO-NO-O_2 Mixtures[a)]

Irradiation time/min	$[C_3H_7CHO]/10^{-7}$ mol dm^{-3}	$\Phi\{n\text{-}C_3H_7CHO\}$
1.00	1.64	0.140
1.50	2.27	0.130
3.00	3.37	0.128
5.00	7.04	0.120
7.00	8.67	0.106
9.00	9.80	0.093
10.50	10.01	0.080

a) $I_a=7.08\times10^{-5}$ Einsteins/s-mol n-C_4H_9ONO. $[O_2]=5.41\times10^{-3}$ mol dm^{-3}. $[NO]=(1.61\pm0.05)\times10^{-6}$ mol dm^{-3}. $T=23$ °C. $[n\text{-}C_4H_9ONO]=(2.76\pm0.05)\times10^{-4}$ mol dm^{-3}.

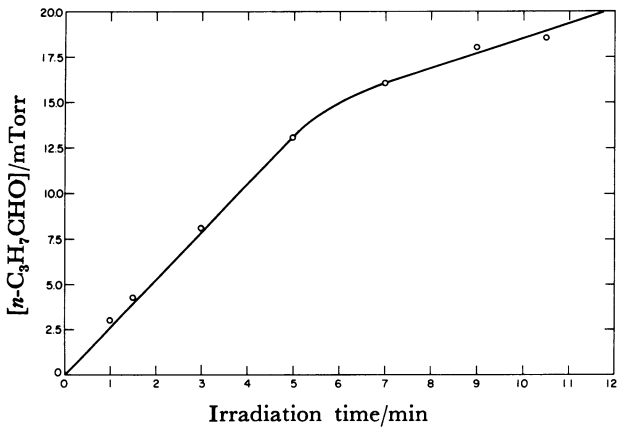

Fig. 1. Plot of $[n\text{-}C_3H_7CHO]$ vs. irradiation time at 23 °C for data in Table 3.

$\Phi\{CH_3CHO\}$ decreases with increasing O_2 pressure. The results are presented in Table 4.

Finally experiments were performed to check if any higher molecular weight products were being formed from the isomerization pathway. In these experiments n-C_4H_9ONO and NO were kept constant at ≃5.0 Torr and ≃30 mTorr, respectively, while the O_2 pressure was varied from 30 to 300 Torr. The total pressure in each experiment was kept constant at 400 Torr with N_2. Continuous recording of the mass spectra in the range of m/z 65—130 was obtained by allowing the contents of the cell to bleed through a small pinhole

Table 4. Photolysis of n-C_4H_9ONO-NO-O_2 Mixtures[a]

$[O_2]/10^{-4}$ mol dm^{-3}	$[NO]/10^{-7}$ mol dm^{-3}	Irradiation time/min	$\Phi\{CH_3CHO\}$	$\Phi\{C_2H_5CHO\}$	$\Phi\{n$-$C_3H_7CHO\}$	$\frac{(\Phi\{n\text{-}C_3H_7CHO\}_{corr}-\rho)^{b)}}{\Phi\{C_2H_5CHO\}_{corr}}$
		$T=-8$ °C, low temp cell, $I_a=6.87\times10^{-5}$ Einsteins/s-mol n-C_4H_9ONO				
16.9	21.3	5.00	—	0.017	0.066	1.35
30.4	18.3	5.00	—	0.016	0.073	1.19
45.5	19.4	4.50	—	0.023	0.110	2.03
60.6	18.8	4.00	—	0.026	0.130	2.13
75.7	18.3	4.00	—	0.029	0.159	2.65
91.0	18.8	3.00	—	0.031	0.174	2.65
106.1	19.9	3.00	—	0.028	0.192	3.36
121.2	18.3	2.50	—	0.032	0.212	3.28
		$T=23$ °C, high temp cell, $I_a=7.08\times10^{-5}$ Einsteins/s-mol n-C_4H_9ONO				
13.6	16.4	4.00	$\leqslant$0.01	0.024	0.064	1.84
19.4	16.4	4.00	$\leqslant$0.01	0.039	0.077	1.35
27.1	16.8	4.00	$\leqslant$0.01	0.030	0.085	1.84
40.7	16.6	4.00	$\leqslant$0.01	0.031	0.092	1.93
54.1	17.3	4.00	$\leqslant$0.01	0.046	0.115	1.52
81.2	16.4	4.00	$\leqslant$0.01	0.045	0.123	1.41
108.3	15.9	4.00	$\leqslant$0.01	0.045	0.151	1.65
		$T=55$ °C, high temp cell, $I_a=1.08\times10^{-4}$ Einsteins/s-mol n-C_4H_9ONO				
12.3	15.1	4.00	0.048	0.048	0.048	0.72
12.3	15.1	4.00	0.050	0.053	0.057	0.86
24.4	15.6	4.00	0.037	0.062	0.068	0.83
36.7	15.1	4.00	0.035	0.067	0.086	0.93
48.8	15.6	4.00	0.035	0.062	0.094	1.05
61.1	15.1	4.00	0.034	0.068	0.099	0.95
61.1	15.1	4.00	0.036	0.069	0.097	0.89
73.2	15.6	4.00	0.031	0.070	0.107	0.97
73.2	16.6	4.00	0.029	0.063	0.105	1.04
85.5	15.1	4.00	0.025	0.069	0.113	1.01
85.1	15.1	4.00	0.026	0.060	0.109	1.12
97.1	15.1	4.00	0.023	0.062	0.119	1.23
97.1	19.1	4.00	0.024	0.062	0.115	1.06
		$T=88$ °C, high temp cell, $I_a=1.10\times10^{-4}$ Einsteins/s-mol n-C_4H_9ONO				
11.1	13.8	4.50	0.134	0.047	0.039	0.70
22.2	13.8	4.00	0.107	0.061	0.059	0.87
33.2	13.8	4.00	0.101	0.075	0.078	0.88
44.3	14.1	4.00	0.075	0.077	0.086	0.97
55.5	13.8	4.00	0.062	0.080	0.092	0.97
66.6	14.1	4.00	0.072	0.093	0.101	0.91
88.7	13.8	4.00	0.069	0.091	0.110	0.98
		$T=120$ °C, high temp cell, $I_a=1.14\times10^{-4}$ Einsteins/s-mol n-C_4H_9ONO				
10.3	1.31	4.00	0.205	0.031	0.030	0.94
20.4	1.23	4.00	0.155	0.045	0.044	0.95
30.7	1.27	4.00	0.150	0.059	0.065	1.07
40.8	1.23	4.00	0.133	0.066	0.078	1.18
51.1	1.27	4.00	0.126	0.068	0.082	1.18
61.3	1.31	4.00	0.121	0.076	0.087	1.10
81.7	1.18	4.00	0.113	0.082	0.093	1.08

a) All runs at 400 Torr total pressure (mainly O_2 and N_2). b) $\rho\equiv(k_{2b}[NO]+k_6[O_2])/k_4$.

into the mass spectrometer. Other techniques such as GC/CI mass spectrometry and high resolution mass spectrometry were also utilized to determine any higher molecular weight products. In all cases the only mass spectral peak that grew was the 76 m/z peak. Relative quantum yields were obtained by assuming a calibration factor since we could not determine the identity of the 76 m/z peak. The results are presented in Table 5 and indicate that $\Phi\{76\}$, the relative quantum yield of the product with m/z 76, remains nearly constant as the O_2 pressure increases at lower temperatures. However at 120 °C, $\Phi\{76\}$ drops as the O_2 pressure increases.

Discussion

O_2 Absent. The mechanism for the photolysis of n-C_4H_9ONO–NO mixtures is:

Table 5. Effect on 76 m/z Peak in the Photolysis of n-C_4H_9ONO-NO-O_2 Mixture[a)]

$[O_2]$/Torr	$\Phi\{76\}$[b)]
$T=23$ °C, $I_a=1.88\times10^{-4}$ Einsteins/s-mol n-C_4H_9ONO	
30	0.262
30	0.270
100	0.330
300	0.277
$T=55$ °C, $I_a=1.88\times10^{-4}$ Einsteins/s-mol n-C_4H_9ONO	
30	0.154
100	0.167
100	0.142
300	0.133
$T=88$ °C, $I_a=1.88\times10^{-4}$ Einsteins/s-mol n-C_4H_9ONO	
30	0.101
100	0.088
300	0.081
$T=120$ °C, $I_a=1.88\times10^{-4}$ Einsteins/s-mol n-C_4H_9ONO	
30	0.091
30	0.097
100	0.070
100	0.064
300	0.048
300	0.048

a) $[n\text{-}C_4H_9ONO]=5.0$ Torr. $[NO]\simeq30$ mTorr. N_2 added to give a total pressure of 400 Torr. b) Relative quantum yield for product with m/z 76.

$$n\text{-}C_4H_9ONO + h\nu \longrightarrow n\text{-}C_4H_9O\cdot + NO, \quad (1)$$

$$n\text{-}C_4H_9O\cdot + NO \longrightarrow n\text{-}C_4H_9ONO, \quad (2a)$$

$$\longrightarrow n\text{-}C_3H_7CHO + HNO, \quad (2b)$$

$$2HNO \longrightarrow N_2O + H_2O, \quad (3)$$

$$n\text{-}C_4H_9O\cdot \longrightarrow I\cdot, \quad (4a)$$

$$\longrightarrow \text{Decomposition}, \quad (4b)$$

$$R\cdot + NO \longrightarrow RNO, \quad (5)$$

where I· is the $HOCH_2CH_2CH_2CH_2\cdot$ radical resulting from the internal abstraction of an H atom by the n-$C_4H_9O\cdot$ radical, and R· can be I· or any radical produced in Reaction 4b.

In addition, there is the possibility that vibrationally-excited n-$C_4H_9O\cdot$ radicals are being produced by photolysis. McMillan et al.[21] have shown that the production of these "hot" alkoxyl radicals is probably not very important in the photolysis of alkyl nitrites at 366 nm. If present, these hot radicals would be expected to rapidly decompose to yield the same products as in the decomposition of the thermally-equilibrated alkoxyl radicals, Reaction 4b.

The data in Table 1 indicate that at 23 °C there is no change in $\Phi\{n\text{-}C_3H_7CHO\}$ with an increase in total pressure. This leads to the conclusion that Reaction 2a is in its second-order regime at our working pressures (>5 Torr) and that "hot" alkoxyl radicals are not present to any significant extent in this sytem.

The Arrhenius expression for k_{4a} has been estimated to be $k_{4a}=10^{11.8}\exp\{-8900/RT\}\ s^{-1}$ by Carter et al.[16] and $k_{4a}=10^{11.4}\exp\{-7700/RT\}\ s^{-1}$ by Baldwin and Golden[17], where the activation energies are in cal mol^{-1}. As we will show our result is in good agreement with these estimates. No measurement exists for k_{4b}, but Baldwin and Golden[17] estimate a high-pressure value for $k_{4b}=10^{13.6}\exp\{-19100/RT\}\ s^{-1}$. Furthermore Batt[22] has reported that for a series of alkoxyl radical decompositions $\log(A_\infty\ s^{-1})$ is $\simeq15$ with high-pressure activation energies $\geqslant13.8$ kcal mol^{-1}. Thus Reaction 4b is very much slower than Reaction 4a at temperatures $\leqslant120$ °C and can be neglected.

The reaction mechanism then predicts that

$$\Phi\{n\text{-}C_3H_7CHO\}^{-1} = \frac{k_2}{\phi_1 k_{2b}}\left(1+\frac{k_2}{k_2[NO]}\right). \quad (a)$$

Plots of $\Phi\{n\text{-}C_3H_7CHO\}^{-1}$ vs. $[NO]^{-1}$ are given in

Table 6. Values of k_4/k_2 at Various Temperatures[a)]

Temp/°C	Intercept[b)]	Slope/Torr[b)]	k_4/k_2/Torr	k_4/k_2/mol dm^{-3}
−8	18.10±0.66	0.72±0.05	0.040±0.004	$(2.39\pm0.25)\times10^{-6}$
23	18.52±0.90	2.95±0.12	0.159±0.010	$(8.60\pm0.55)\times10^{-6}$
55	20.74±5.93	9.40±0.90	0.452±0.140	$(2.21\pm0.68)\times10^{-5}$
88	21.95±6.70	34.0±1.7	1.55 ±0.80	$(6.87\pm3.55)\times10^{-5}$
120	19.11±4.94	210±10	11.1 ±3.2	$(4.52\pm1.31)\times10^{-4}$

a) Uncertainties are one standard deviation. b) From Figs. 2—4.

Figs. 2—4 for the five temperatures studied. The plots are linear, and the intercepts and slopes are listed in Table 6. The slope increases with increasing temperature while the intercept remains essentially constant at 20.0±2.0. The data at 23 and 120 °C were taken to much higher values of [NO] than at the other temperatures and should give more reliable values for the intercept. However the uncertainty at 120 °C is quite large. Thus we adopt the value of 18.5 obtained at 23 °C for the intercept, independent of temperature. The intercept gives $k_2/k_{2b}\phi_1$. Previously we have shown that $k_{2b}/k_2=0.29\pm0.05$.[20] Thus $\phi_1=0.19\pm0.04$. The ratio of slope to intercept gives k_4/k_2 and these values are given in Table 6. An Arrhenius plot for k_4/k_2 is shown in Fig. 5. The data show some curvature, but the least-squares straight line gives $\ln(k_4/k_2,\ \mathrm{mol\ dm^{-3}})=1.93\pm1.60-(4014\pm509)/T$. A value of k_2 has never been determined for butoxyl, but Batt[22] has shown that k_2 is essentially constant and independent of temperature for a series of alkoxyl radicals from methoxyl to *t*-pentoxyl. His value for k_2 for the ethoxyl radical is 2.6×10^{10} dm^3 mol^{-1} s^{-1}. With this value for k_2, $\log(k_4,\ \mathrm{s^{-1}})=11.25\pm0.69-(4014\pm509)/2.303T$. Our activation energy of 8.0 kcal mol^{-1} is in good agreement with the estimates of 8.9[16] and 7.7[17] kcal mol^{-1}, while our pre-exponential factor of 11.25 is somewhat lower than the estimates of 11.8[16] and 11.4[17].

O_2 Present. In the presence of O_2, the following additional reactions occur.

$$n\text{-}C_4H_9O\cdot + O_2 \longrightarrow n\text{-}C_3H_7CHO + HO_2\cdot \quad (6)$$

$$HO_2\cdot + NO \longrightarrow NO_2 + HO\cdot \quad (7)$$

$$HO\cdot + n\text{-}C_4H_9ONO \longrightarrow H_2O + n\text{-}C_3H_7CHO + NO \quad (8a)$$

$$\longrightarrow n\text{-}C_4H_9O\cdot + HONO \quad (8b)$$

$$\longrightarrow \text{Termination } (+76) \quad (8c)$$

$$\longrightarrow \text{Termination } (-76) \quad (8d)$$

$$HO\cdot + NO + M \longrightarrow HONO + M \quad (9)$$

$$HO\cdot + NO_2 + M \longrightarrow HONO_2 + M \quad (10)$$

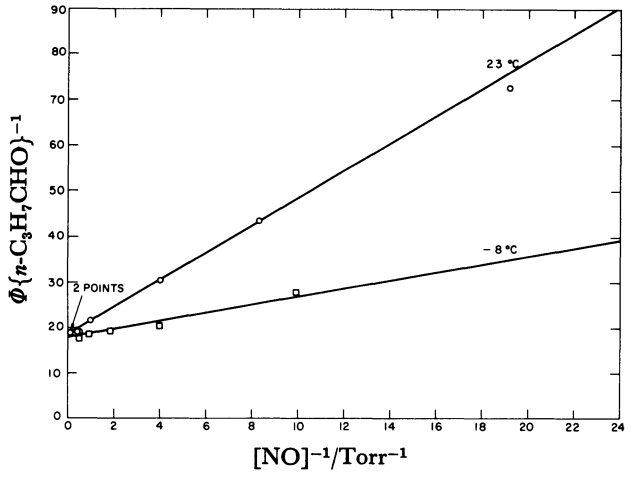

Fig. 2. Plots of $\Phi\{n\text{-}C_3H_7CHO\}^{-1}$ vs. $[NO]^{-1}$ at temperatures of −8 and 23 °C.

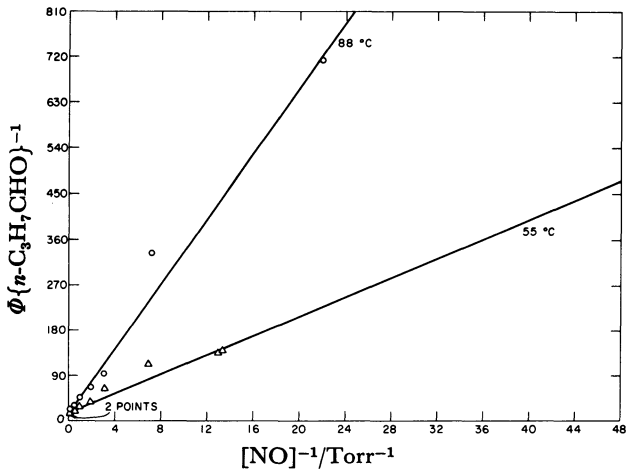

Fig. 3. Plots of $\Phi\{n\text{-}C_3H_7CHO\}^{-1}$ vs. $[NO]^{-1}$ at temperatures of 55 and 88 °C.

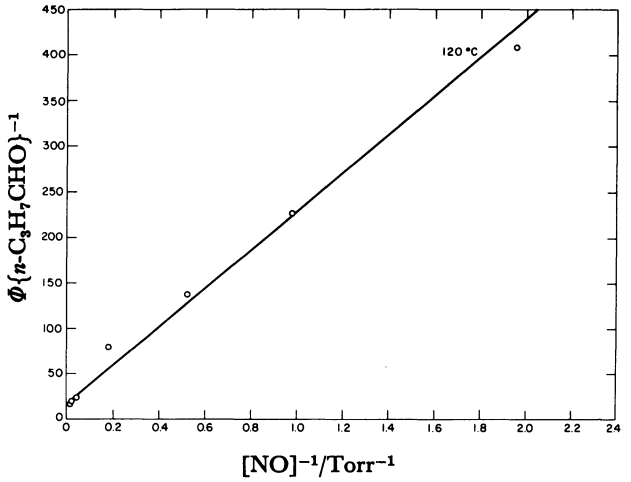

Fig. 4. Plot of $\Phi\{n\text{-}C_3H_7CHO\}^{-1}$ vs. $[NO]^{-1}$ at 120 °C.

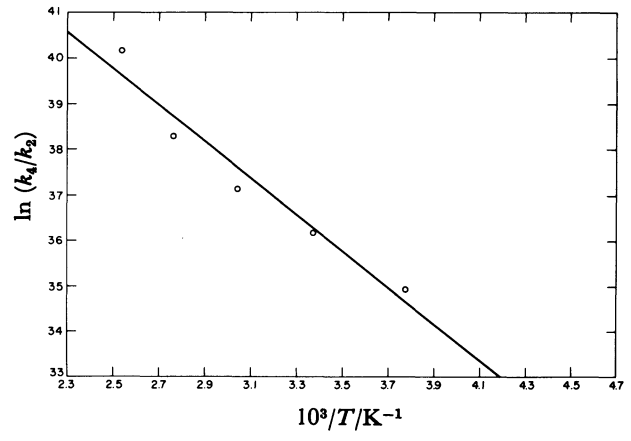

Fig. 5. Arrhenius plot for k_4/k_2.

$$n\text{-}C_4H_9O\cdot + NO_2 \longrightarrow n\text{-}C_4H_9ONO_2 \quad (11a)$$
$$\longrightarrow n\text{-}C_3H_7CHO + HONO, \quad (11b)$$

where Reactions 8c and 8d are some unspecified radical termination steps that either produce the high-molecular weight product with m/z 76 (Reaction 8c) or do not produce it (Reaction 8d). Some termination steps are required in Reaction 8 since other termination steps are too slow to account for the results. We believe that the unidentified product with m/z 76 may be formed in a termination step since its quantum yield is independent of O_2 pressure (except at 120 °C). In principle the reaction of $HO_2\cdot$ with NO_2 should be included, but it is very much slower than Reaction 7 under our reaction conditions so that it can be ignored.

The rate coefficients at 23 °C for k_9 and k_{10} are, respectively, 2.4×10^{11} dm^3 mol^{-1} s^{-1} and 9.4×10^{11} dm^3 mol^{-1} s^{-1} [23] for N_2 or O_2 as a chaperone. k_8 has been measured for butyl nitrite, and it is 2.9×10^9 dm^3 mol^{-1} s^{-1} at 295 K.[24] Furthermore k_8, k_9, and k_{10} are not very sensitive to temperature changes. Thus under all of our conditions 98% of the HO· radicals react with n-C_4H_9ONO, and Reactions 9 and 10 can be ignored. In principal Reaction 11 must be included in the reaction scheme, since NO is converted to NO_2, but Reaction 11 behaves just like Reaction 2, so that ignoring it does not affect the analysis.

The fate of the radical I· formed in Reaction 4b must be considered. It must lead to the aldehyde products which are observed. $\Phi\{CH_3CHO\}$ decreases but $\Phi\{C_2H_5CHO\}$ and $\Phi\{n\text{-}C_3H_7CHO\}$ increase with increasing O_2 pressure. Thus a competition exists to produce these aldehydes, and the implied reactions are

$$I\cdot \longrightarrow CH_3CHO + 2CH_2O + HO, \quad (12a)$$
$$\longrightarrow \text{Undetected aldehydes} + HO, \quad (12b)$$
$$I\cdot + O_2 \longrightarrow n\text{-}C_3H_7CHO + HO, \quad (13a)$$
$$\longrightarrow C_2H_5CHO + HO, \quad (13b)$$

where all the reactions are composite reactions. It is not clear how Reaction 12 proceeds. It may involve an internal rearrangement, a bond cleavage, or reaction with NO. Reaction 12b is included for generality, and appears to be needed. The undetected aldehydes may be $CH_2O\cdot$ or other carbonyl compounds. A corresponding reaction could be written for the I·+O_2 reaction, and it may occur to some extent. However for simplicity we shall ignore it.

Reaction 13a probably proceeds via

$$I\cdot + O_2 \longrightarrow HO_2\cdot + \cdot OCH_2CH_2CH_2CH_2\cdot$$

followed by Reaction 7 and rearrangement of the diradical to give n-C_3H_7CHO. The rearrangement may proceed through an excited cyclic tetrahydrofuran intermediate. Reaction 13b probably occurs by addition of O_2 to the radical site

$$I\cdot + O_2 \longrightarrow HOCH_2CH_2CH_2CH_2O_2\cdot$$

followed by

$$HOCH_2CH_2CH_2CH_2O_2\cdot + NO \longrightarrow HOCH_2CH_2CH_2CH_2O\cdot + NO_2$$
$$HOCH_2CH_2CH_2CH_2O\cdot \longrightarrow HOCH_2CH_2CH_2\cdot + CH_2O$$
$$HOCH_2CH_2CH_2\cdot + O_2 \longrightarrow HO_2\cdot + \cdot OCH_2CH_2CH_2\cdot$$

followed by Reaction 7 and rearrangement of the diradical to C_2H_5CHO.

At 120 °C, the ratio $\Phi\{n\text{-}C_3H_7CHO\}/\Phi\{C_2H_5CHO\}$ is constant at 1.40±0.07 independent of O_2 pressure. This indicates that all of the n-C_3H_7CHO is produced in reaction 13a, and that neither Reactions 6 nor 8a are important at 120 °C. Since Reactions 8a and 8b both have small and similar activation energies, then if Reaction 8a is unimportant at 120 °C, it will also be unimportant at all temperatures. This differs markedly from the situation with the lower alkyl nitrites, where it was found that Reactions 8a and 8b were of comparable importance at all temperatures.[11-13] Reaction 8a is really a two-step reaction; i.e. an H-atom abstraction followed by a decomposition of the resulting radical. Possibly with n-C_4H_9ONO, the radical formed from the abstraction isomerizes and undergoes further oxidation before decomposition. Thus Reaction 8a transforms into Reactions 8c and 8d.

The mechanism predicts that

$$\frac{\phi_1(k_{2b}[NO]+\varepsilon k_4+k_6[O_2])}{\sum\Phi\{ald\}(k_2[NO]+k_4+k_6[O_2])} = \frac{(k_{8c}+k_{8d}+\Gamma k_{8b})}{k_8} \quad (b)$$

where $\Gamma \equiv k_2[NO]/(k_2[NO]+k_4+k_6[O_2])$

$\varepsilon \equiv (k_{12a}+k_{13}[O_2])/(k_{12}+k_{13}[O_2])$

$\sum\Phi\{ald\} \equiv \Phi\{CH_3CHO\} + \Phi\{C_2H_5CHO\} + \Phi\{n\text{-}C_3H_7CHO\}$

At 120 °C, $\sum\Phi\{ald\}=0.27\pm0.01$ independent of O_2 pressure. This means that k_{12b} is unimportant so that $\varepsilon=1.0$, and that Reaction 2 is negligible compared to Reaction 4. Γ is essentially zero, and Eq. b simplifies to

$$\phi_1/\sum\Phi\{ald\} = (k_{8c}+k_{8d})/k_8. \quad (c)$$

Since $\phi_1=0.19$, $(k_{8c}+k_{8d})/k_8=0.70\pm0.03$ at 120 °C. At lower temperatures, the correction terms become more important, but they are still small at 88 °C. Here $\sum\Phi\{ald\}$ increases from 0.22 at low $[O_2]$ to 0.27 at high $[O_2]$ indicating that ε is not constant. However at high $[O_2]$, $\varepsilon\simeq1.0$, and Eq. c can be used. Thus at 88 °C, $(k_{8c}+k_{8d})/k_8$ also is $\simeq0.70$. This is in accord with the findings for lower alkyl nitrites that the branching ratios for k_8 are independent of temperature.[11-13] Thus we assume that $(k_{8c}+k_{8d})/k_8=0.70$ at

all temperatures and thus $k_{8b}/k_8=0.30$. This can be compared with the values of 0.57±0.13, 0.44±0.24, and 0.66±0.12 found, respectively, for $C_2H_5O\cdot$,[11] n-$C_3H_7O\cdot$,[12] and i-$C_4H_9O\cdot$.[13]

The mechanism gives a rate law for butyraldehyde production which can be cast into two forms:

$$(\Phi\{n\text{-}C_3H_7CHO\}_{corr}-\rho)^{-1}=\frac{k_{13}}{k_{13a}}+\frac{k_{12}}{k_{13a}[O_2]}, \quad (d)$$

$$\Phi\{n\text{-}C_3H_7CHO\}_{corr}-\frac{k_{2b}[NO]}{k_4}-\frac{k_{13a}[O_2]}{(k_{12}+k_{13}[O_2])}=\frac{k_6[O_2]}{k_4}, \quad (e)$$

where $\Phi\{n\text{-}C_3H_7CHO\}_{corr}\equiv\theta\Phi\{n\text{-}C_3H_7CHO\}/\phi_1\xi$

$\rho\equiv(k_{2b}[NO]+k_6[O_2])/k_4$

$\theta\equiv(\Gamma k_{8b}+k_{8c}+k_{8d})/k_8$

$\xi\equiv k_4/(k_2[NO]+k_4+k_6[O_2])$.

All of the rate coefficient ratios needed to compute the parameters in Eqs. d and e are known except for k_6/k_4, k_{12}/k_{13a}, and k_{13}/k_{13a}. Thus at each temperature we assume a value for k_6/k_2, compute the left-hand-side of Eq. d, and plot it vs. $[O_2]^{-1}$. From the slope and intercept of the plot, we obtain k_{12}/k_{13a} and k_{13}/k_{13a}, respectively. These values are then used to compute the left-hand-side of Eq. e, which is then plotted vs. $[O_2]^{-1}$ to get a new value for k_6/k_4. This value is then used for the next calculation of the parameters in Eq. d, and the process is repeated until consistent values of k_6/k_4, k_{13}/k_{13a}, and k_{12}/k_{13a} are obtained. This method works well at all temperatures except at −8 and 120 °C. At 120 °C, Eq. e fails because Reaction 6 makes a negligible contribution to $\Phi\{n\text{-}C_3H_7CHO\}$ under all conditions. At this temperature k_6/k_2 is obtained from an extrapolation of the Arrhenius plot of the values at lower temperatures. At −8 °C, Eq. d fails because the results suggest an excess production of n-C_3H_7CHO not accounted for in the mechanism. At this temperature k_{12}/k_{13a} and k_{13}/k_{13a} are obtained from an extrapolation of their Arrhenius plots of the values at higher temperatures.

The final plots based on Eqs. d and e are shown in Figs. 6 and 7, respectively, at each temperature. The values of the slopes and intercepts are listed in Table 7. The intercepts of Fig. 7 have been forced to zero as predicted. Regression analyses of the Arrhenius plots (not shown) give the Arrhenius expressions tabulated in Table 8. If k_2 is taken to be 4.4×10^{-11} cm^3 s^{-1},[22] then $k_6=4.5\times10^8\exp\{(-1178\pm176)/T\}$ dm^3 mol^{-1} s^{-1}. Both the pre-exponential factor and activation energy are slightly larger than those found for the lower alkoxyl radicals.[11-13] However, this difference probably just represents uncertainties since k_6 was determined over a small temperature range (23—88 °C) in this study.

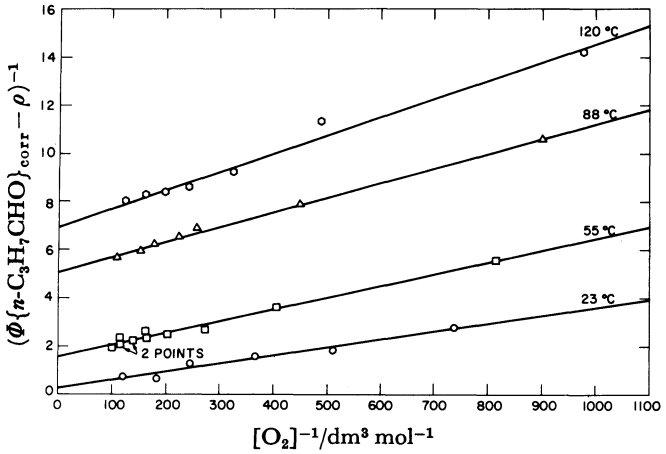

Fig. 6. Plots of $(\Phi\{n\text{-}C_3H_7CHO\}_{corr}-\rho)^{-1}$, computed using values of k_6/k_2 in Table 7, vs. $[O_2]^{-1}$. The plots are displaced upwards by 5, 3, −1, and −2 units, respectively, for 120, 88, 55, and 23 °C for clarity.

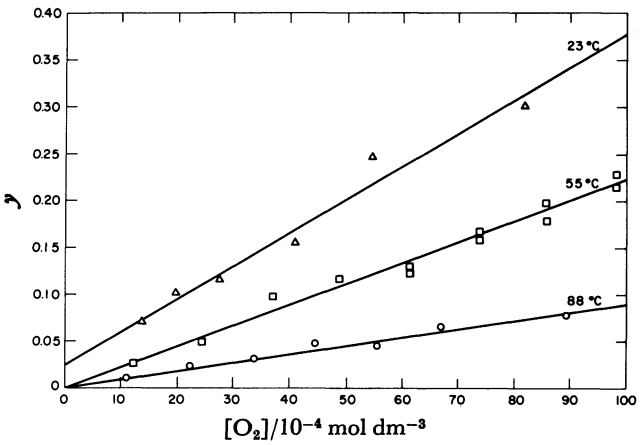

Fig. 7. Plots of y=left-hand side of Eq. e as computed using values of k_{13a}/k_{13} and k_{13a}/k_{12} in Table 7, vs. $[O_2]$. The plot at 23 °C is dispaced upward by 0.025 unit for clarity.

Table 7. Rate Coefficient Ratios from $\Phi\{n\text{-}C_3H_7CHO\}$ Analysis[a,b]

Temp/°C	$10^3\,k_{12}/k_{13a}$/mol dm^{-3}	k_{13a}/k_{13}	$10^3\,k_{12}/k_{13}$/mol dm^{-3}	k_6/k_2
−8	2.29[c]	0.38[c]	0.88[c]	1.97×10^{-4} [c]
23	3.37±0.30	0.444±0.016	1.49±0.22	$(3.05\pm0.20)\times10^{-4}$
55	4.90±0.17	0.394±0.080	1.93±0.30	$(4.92\pm0.17)\times10^{-4}$
88	6.19±0.15	0.489±0.050	3.02±0.18	$(6.21\pm0.40)\times10^{-4}$
120	7.57±0.45	0.508±0.052	3.85±0.23	$(8.35\pm0.55)\times10^{-4}$ [c]

a) Uncertainties are one standard deviation. b) Results tabulated using $k_{8b}/k_8=0.30$. c) Values were determined by extrapolation from Arrhenius plots.

A simpler analysis is obtained from examination of C_2H_5CHO production. The rate law for $\Phi\{C_2H_5CHO\}$ is

$$\Phi\{C_2H_5CHO\}_{corr}^{-1} = \frac{k_{13}}{k_{13b}} + \frac{k_{12}}{k_{13b}[O_2]}, \qquad (f)$$

where

$$\Phi\{C_2H_5CHO\}_{corr} \equiv \Phi\{C_2H_5CHO\}\theta/\phi_1\xi.$$

The left-hand-side of Eq. f is computed from the rate coefficient ratios already determined including those for k_6/k_2, though reaction 6 makes only a trivial correction. The left-hand side of Eq. f is plotted vs. $[O_2]^{-1}$ in Figs. 8 and 9. The values of k_{13b}/k_{13}, k_{12}/k_{13b}, and k_{12}/k_{13} obtained from the plots are listed in Table 9. Respective Arrhenius parameters are listed in Table 8.

The sum of $k_{13a}/k_{13}+k_{13b}/k_{13}$ should be 1.0 according to the mechanism. It is listed in Table 10 and varies from 0.74 to 0.90, indicating that another channel to Reaction 13, perhaps giving CH_2O, might also occur. The ratio k_{13a}/k_{13b} found from the individual values of k_{13a}/k_{13} and k_{13b}/k_{13} is also listed in Table 10. It is about 1.3 independent of temperature.

Another way to obtain k_{13a}/k_{13b} is directly from the following equation predicted by the mechanism:

$$(\Phi\{n\text{-}C_3H_7CHO\}_{corr} - \rho)/\Phi\{C_2H_5CHO\}_{corr} = k_{13a}/k_{13b} \qquad (g)$$

The values of the left-hand side of Eq. g are listed in

Table 8. Regression Equations[a)]

A) From $\Phi\{n\text{-}C_3H_7CHO\}$ analysis
$\ln(k_{13a}/k_{13}) = -0.17\pm0.49-(209\pm165)/T$
$\ln(k_{13a}/k_{12}) = -2.42\pm0.15+(963\pm49)/T$
$\ln(k_{12}/k_{13}) = -2.61\pm0.36-(1194\pm66)/T$
$\ln(k_6/k_2) = -4.09\pm0.54-(1178\pm176)/T$

B) From $\Phi\{C_2H_5CHO\}$ analysis
$\ln(k_{13b}/k_{13}) = -0.60\pm0.41-(139\pm131)/T$
$\ln(k_{12}/k_{13b}) = -6.35\pm1.77+(324\pm566)/T$
$\ln(k_{12}/k_{13}) = -7.12\pm1.87+(230\pm597)/T$

C) Others
$\ln(k_4/k_2) = 1.92\pm1.60-(4014\pm509)/T$[b)]
$\ln(k_{13a}/k_{13b}) = -2.03\pm0.68+(738\pm217)/T$[c)]

a) Uncertainties are 1 standard deviation. Units of rate coefficient ratios are in mol dm^{-3} to the appropriate power. b) From data in absence of O_2. c) From mean values listed in Table 10.

Table 9. Rate Coefficient Ratios from $\Phi\{C_2H_5CHO\}$ Analysis[a,b)]

Temp/°C	k_{13b}/k_{13}	$10^3\,k_{12}/k_{13b}$/ mol dm^{-3}	$10^3\,k_{12}/k_{13}$/ mol dm^{-3}
−8	0.361±0.074	7.01±1.99	2.52±0.17
23	0.295±0.079	6.22±2.17	1.96±0.12
55	0.334±0.010	2.16±0.23	7.31±0.10
88	0.413±0.022	3.82±0.30	1.39±0.12
120	0.385±0.016	6.33±0.25	2.42±0.12

a) Uncertainties are one standard deviation. b) Results tabulated using $k_{8b}/k_8 = 0.30$.

Table 10. Comparison of k_{13a}/k_{13} and k_{13b}/k_{13}

Temp/°C	$(k_{13a}+k_{13b})/k_{13}$[a)]	k_{13a}/k_{13b}[b)]	k_{13a}/k_{13b}[c)]
−8	0.74	1.06	2.32±0.81
23	0.74	1.51	1.65±0.25
55	0.73	1.18	0.97±0.11
88	0.90	1.18	0.90±0.10
120	0.89	1.32	1.07±0.10

a) Sum of values obtained individually from $\Phi\{n\text{-}C_3H_7CHO\}$ and $\Phi\{C_2H_5CHO\}$ as listed in Tables 7 and 9, respectively b) Ratio of values obtained individually from $\Phi\{n\text{-}C_3H_7CHO\}$ and $\Phi\{C_2H_5CHO\}$ as listed in Tables 7 and 9, respectively. c) Obtained from mean value of k_{13a}/k_{13b} obtained from $(\Phi\{n\text{-}C_3H_7CHO\}_{corr}-\rho)/\Phi\{C_2H_5CHO\}_{corr}$ from Table 4.

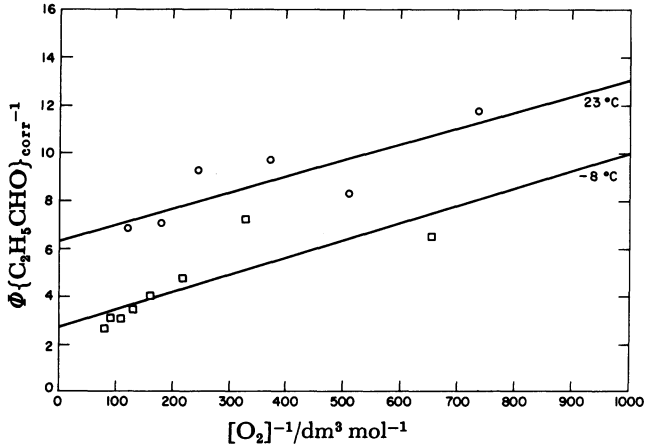

Fig. 8. Plots of $\Phi\{C_2H_5CHO\}_{corr}^{-1}$ computed using values of k_6/k_2 in Table 7, vs. $[O_2]^{-1}$ at −8 and 23 °C. The plot at 23 °C is displaced upward by 3 units for clarity.

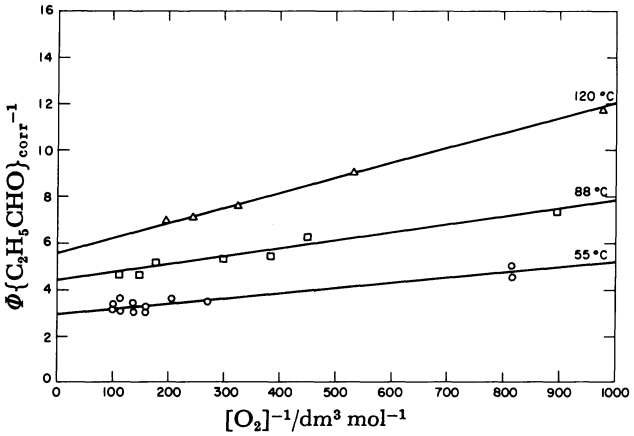

Fig. 9. Plots of $\Phi\{C_2H_5CHO\}_{corr}^{-1}$, computed using values of k_6/k_2 in Table 7, vs. $[O_2]^{-1}$ at 55, 88, and 120 °C. The plots at 88 and 120 °C are displaced upward by 2 and 3 units, respectively, for clarity.

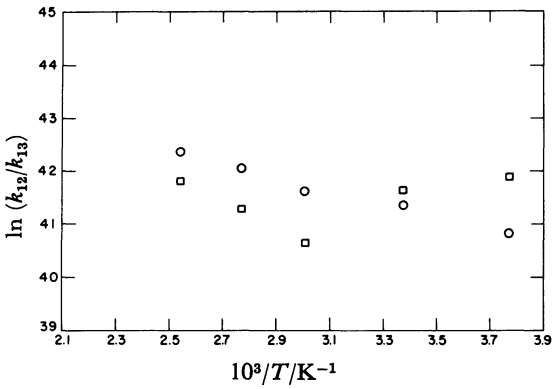

Fig. 10. Arrhenius plot for $\ln(k_{12}/k_{13})$ vs. reciprocal temperature.
○, from $\Phi\{n\text{-}C_3H_7CHO\}$; and □, from $\Phi\{C_2H_5CHO\}$.

Table 4 for every run. The values are nearly independent of O_2 pressure, as they should be, except at −8 °C, where they increase with $[O_2]$. It is not clear why this trend occurs at −8 °C, but an additional source of n-C_3H_7CHO, not given by the mechanism, is indicated. The mean values at any temperature are listed in Table 10, and they are consistent with the values obtained from analysis of the individual aldehyde quantum yields.

In principle additional information can be found from the rate law for CH_3CHO formation. However this is not feasible here since the details of the rate law are unknown. The values of k_{12}/k_{13} obtained from $\Phi\{n\text{-}C_3H_7CHO\}$ and $\Phi\{C_2H_5CHO\}$ are plotted in an Arrhenius plot in Fig. 10. The agreement between the values obtained from the two aldehydes is good only to within a factor of three. The values obtained from $\Phi\{n\text{-}C_3H_7CHO\}$ give a good linear Arrhenius plot, whereas those from $\Phi\{C_2H_5CHO\}$ do not. Thus we prefer the value of k_{12}/k_{13} obtained from $\Phi\{n\text{-}C_3H_7CHO\}$.

For the quantum yield of termination product of Reaction 8c, $\Phi\{76\}$, the mechanism predicts that

$$\Phi\{76\} = \phi_1(1-\Gamma)k_{8c}/(k_{8c}+k_{8d}+\Gamma k_{8b}\} . \qquad (i)$$

Since $\Gamma \simeq 0$, Eq. i simplifies to:

$$\Phi\{76\} = \phi_1 k_{8c}/(k_{8c}+k_{8d}) . \qquad (j)$$

Thus $\Phi\{76\}$ should be independent of O_2 pressure at any temperature, which it is, except at 120 °C. Perhaps at 120 °C, some secondary oxidation of this product occurs which reduces its primary quantum yield. However it decreases with increasing temperature indicating that both Reaction 8c and 8d must be playing a role in termination. Since only relative values are known for $\Phi\{76\}$, the relative importance of Reactions 8c and 8d cannot be found.

We appreciate helpful comments and suggestions by S. Zabarnick. This work was supported by the Environmental Protection Agency through Grant. No. R808528 for which we are grateful.

References

1) H. A. Wiebe, A. Villa, T. M. Hellman, and J. Heicklen, *J. Am. Chem. Soc.*, **95**, 7 (1973).
2) W. Glasson, *Environ. Sci. Technol.*, **9**, 1048 (1975).
3) W. A. Alcock and B. Mile, *Combust. Flame*, **24**, 125 (1975).
4) J. R. Barker, S. W. Benson, and D. M. Golden, *Int. J. Chem. Kinet.*, **9**, 31 (1977).
5) L. J. Kirsch and D. A. Parkes, Presented at 5th International Symposium on Gas Kinetics, Manchester, Great Britain, 1977.
6) L. Batt and G. N. Robinson, *Int. J. Chem. Kinet.*, **11**, 1045 (1979).
7) K. Selby and D. J. Waddington, *J. Chem. Soc., Perkin Trans. 2*, **1979**, 1259.
8) R. A. Cox, R. G. Derwent, S. V. Kearsey, L. Batt, and K. G. Patrick, *J. Photochem.*, **13**, 149 (1980).
9) D. Gutman, N. Sanders, and J. E. Butler, *J. Phys. Chem.*, **86**, 66 (1982).
10) L. Batt, K. G. Patrick, and G. A. Reid, Presented at International Symposium on Chemical Kinetics Related to Atmospheric Chemistry, Tsukuba, Ibaraki, Japan (June, 1982), Paper No. 39.
11) S. Zabarnick and J. Heicklen, *Int. J. Chem. Kinet.*, **17**, 455 (1985).
12) S. Zabarnick and J. Heicklen, *Int. J. Chem. Kinet.*, **17**, 477 (1985).
13) S. Zabarnick and J. Heicklen, *Int. J. Chem. Kinet.*, **17**, 503 (1985).
14) A. Fish, *Quart. Rev. Chem. Soc.*, **18**, 243 (1964).
15) A. C. Baldwin, J. R. Barker, D. M. Golden, and D. G. Hendry, *J. Phys. Chem.*, **81**, 2483 (1977).
16) W. P. L. Carter, K. R. Darnall, A. C. Lloyd, A. M. Winer, and J. N. Pitts, Jr., *Chem. Phys. Lett.*, **42**, 22 (1976).
17) A. C. Baldwin and D. M. Golden, *Chem. Phys. Lett.*, **60**, 108 (1978).
18) H. Niki, P. D. Maker, C. M. Savage, and L. P. Breitenbach, *J. Phys. Chem.*, **85**, 2698 (1981).
19) P. Morabito and J. Heicklen, *Int. J. Chem. Kinet.*, **17**, 535 (1985).
20) P. Morabito and J. Heicklen, *J. Phys. Chem.*, **89**, 2914 (1985).
21) G. R. McMillan, J. Kumari, and D. L. Snyder, "Chemical Reactions in Urban Atmospheres," ed by C. S. Tuesday (1971), p. 35.
22) L. Batt, *Int. J. Chem. Kinet.*, **11**, 977 (1979).
23) R. F. Hampson, DOT Report No. FAA-EE-80-17 (1982) "Chemical Kinetic and Photochemical Data Sheets for Atmospheric Reactions."
24) D. L. Baulch, I. M. Campbell, and S. M. Saunders, *Int. J. Chem. Kinet.*, **17**, 355 (1985).